Bionanotechnology

DOI: 10.1002/anie.200805998

All-in-One Target-Cell-Specific Magnetic Nanoparticles for Simultaneous Molecular Imaging and siRNA Delivery**

Jae-Hyun Lee, Kyuri Lee, Seung Ho Moon, Yuhan Lee, Tae Gwan Park, and Jinwoo Cheon**

There has been considerable interest in the development of a variety of functional inorganic nanoparticles that can be applied in biomedical technologies, including nanotherapeutics, diagnostics, biosensors, and medical imaging.[1,2] Of particular significance is the use of magnetic nanoparticles for magnetic resonance imaging (MRI), cell and protein separation, heat generation, and magnetism-induced cellular mechanotransduction.[3,4] The ease of the synthesis of magnetic nanoparticles and subsequent surface modifications to introduce additional therapeutic and diagnostic functionalities has enabled these systems to be employed as smart nanomedicines that incorporate combinations of different components.[5] Various cell-specific targeting, imaging, and therapeutic functions can be incorporated into a single magnetic nanoparticle which is designed for simultaneous diagnostic and therapeutic use, without losing the individual properties of each component.

It is known that synthetic small interfering RNA (siRNA) can inhibit specific protein expression by suppressing a target gene selectively at the posttranscriptional mRNA level by a mechanism called RNA interference (RNAi).[6] siRNAs have been studied extensively to treat various genetic diseases, including cardiovascular diseases and various cancers.[7] The development of appropriate carrier systems is crucial for practical applications of siRNAs as therapeutics. However, many siRNA-carrier systems, including cationic polymers and lipids, possess inherent deficiencies associated with target-cell-specific gene inhibition and biocompatibility.[8,9]

[*] K. Lee,[+] Y. Lee, Prof. T. G. Park
Department of Biological Sciences
Korea Advanced Institute of Science and Technology
Daejeon 305-701 (Korea)
Fax: (+82) 42-869-2610
E-mail: tgpark@kaist.ac.kr

J.-H. Lee,[+] S. H. Moon, Prof. J. Cheon
Department of Chemistry, Yonsei University
Seoul 120-749 (Korea)
Fax: (+82) 2-364-7050
E-mail: jcheon@yonsei.ac.kr

[+] These authors contributed equally.

[**] This research was supported by the National Research Laboratory Program (M10600000255 for J.C. and N01080127 for T.G.P.), AFOSR (FA4869-08-1-4046), NCI Center for Cancer Nanotechnology Excellence (CCNE), NCRC (R15-2004-024-00000-0), the Ministry of Health, Welfare, and Family Affairs (N04080181), the Korea Research Council of Fundamental Science & Technology, and the second-stage BK21 project for chemistry at Yonsei University.

siRNA = small interfering RNA.

Supporting information for this article is available on the WWW under http://dx.doi.org/10.1002/anie.200805998.

A number of inorganic nanocrystalline materials have been emerging as potential siRNA carriers in systems devised for simultaneous imaging and therapeutic purposes.[9b,c] Magnetic nanoparticles are highly attractive platform materials for siRNA delivery owing to their unique properties which include uniform size, biocompatibility, superior imaging characteristics, and facile surface modification. Cell-specific targeting strategies for high-performance magnetic nanoparticles with dual (diagnostic and therapeutic) functions also include the immobilization of various target-specific moieties, such as antibodies, small peptides that can be recognized by cells, and aptamers.[10] In particular, Arg-Gly-Asp (RGD) conjugated nanoparticles bind strongly to $\alpha_v\beta_3$ integrin, which is overexpressed in both endothelial and specific cancer cells, and internalize into the cells by receptor-mediated endocytosis, whereas RGD itself does not promote the endosomal escape of nanoparticles into the cytoplasm.[11]

In this study, we developed "all-in-one" nanoparticle probes for simultaneous delivery and multimodal imaging. The magnetic nanoparticle probes were conjugated with siRNAs, cancer-cell-specific targeting moieties, and fluorescent dyes. Our purpose in designing the multifunctional nanoprobe was to enable highly accurate imaging to be carried out simultaneously with the delivery of therapeutics. This approach is clinically important, as it can minimize invasiveness and deleterious side effects. As a result of the ability of the probes to target specific cells, siRNAs will be unloaded only inside targeted cells with certain receptors; the disulfide linkages between siRNAs and the nanoparticles should be cleaved inside the cells. In principle, it is possible to monitor where the probes with therapeutics are located in the targeted areas. More specifically, magnetic nanoparticles are useful for visualizing the location and trafficking of siRNA for in vivo applications. However, the innate limit of spatial resolution in MRI (ca. 100 μm) makes it impossible to monitor the intracellular transfection of siRNA by MRI. For this reason, the fluorescent dye is required for sensitive subcellular visualization.

For the fabrication of multifunctional magnetic nanoparticles, manganese-doped magnetism-engineered iron oxide (MnMEIO) nanoparticles of 15 nm in size coated with bovine serum albumin (BSA) were used as the core material (Figure 1 a) owing to their high degree of size monodispersity, the ease with which their surface can be modified, and their higher magnetic moment than that of other conventional iron oxide based magnetic nanoparticles.[12] The last property translates into enhanced MRI signals. For bioconjugation and nanoparticle delivery into the cytoplasm of cells, cationized BSA with a pI (isoelectric point) value of 6.1 was used.[13,14] The primary amine groups of

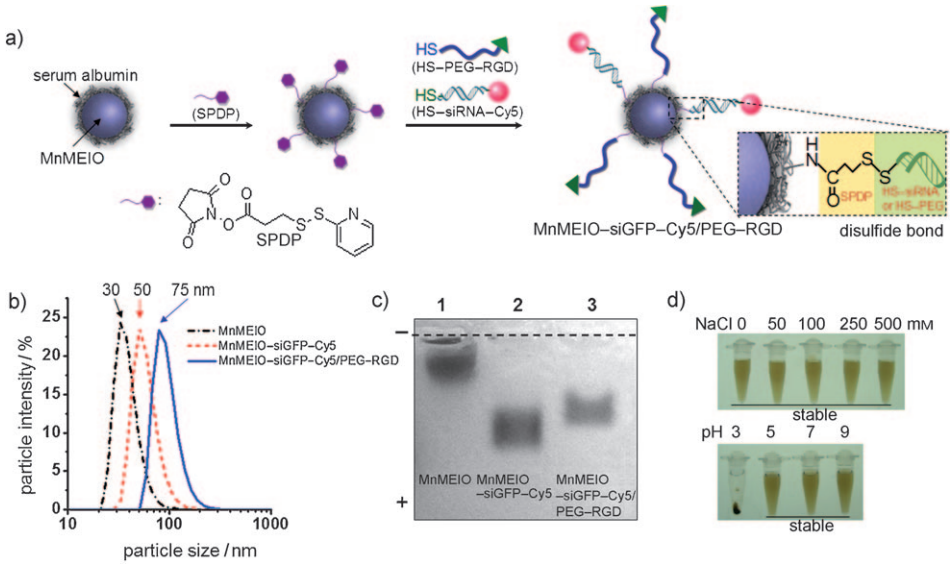

Figure 1. Fabrication of multimodal MnMEIO–siGFP–Cy5/PEG–RGD. a) Synthetic scheme for MnMEIO–siGFP–Cy5/PEG–RGD. SPDP, which forms disulfide bonds, was used as a linker. b) Hydrodynamic diameter of MnMEIO (black dotted line), MnMEIO–siGFP–Cy5 (red dotted line), MnMEIO–siGFP–Cy5/PEG–RGD (blue solid line). c) Agarose-gel electrophoresis showing a negative zeta potential induced by siRNA conjugation (lane 1: MnMEIO; lane 2: MnMEIO–siGFP–Cy5; lane 3: MnMEIO–siGFP–Cy5/PEG–RGD). d) Colloidal-stability test at varying NaCl concentrations and pH values.

BSA on the surface of the MnMEIO nanoparticles were converted into pyridyldisulfide groups by treatment with *N*-succinimidyl-3-(2-pyridyldithio)propionate (SPDP). An Ellman assay revealed that the nanoparticles were activated sufficiently upon reaction with SPDP (ca. 700 SPDP functional groups per particle). The SPDP-activated MnMEIO nanoparticles were then treated with thiolated poly(ethylene glycol) (PEG, MW 3400) functionalized with a cyclic Arg-Gly-Asp (RGD) peptide at the distal end (HS–PEG–RGD). The resulting nanoparticles were treated with Cy5-dye-labeled thiolated siRNA (HS–siGFP–Cy5), which can inhibit the expression of green fluorescence protein (GFP). siRNA molecules were attached to the surface of nanoparticles through disulfide bonds, which could be cleaved readily in an intracellular environment. Arg-Gly-Asp (RGD) peptides are known to bind specifically to $\alpha_v\beta_3$ integrin, which is expressed abundantly in metastatic tumor cells and tumor endothelial cells and is known to play a critical role in receptor-mediated endocytosis.[11]

The constructed nanoparticle (MnMEIO–siGFP–Cy5/PEG–RGD), in which PEGylated RGD is incorporated for both nanoparticle stabilization and cancer-cell targeting and siGFP–Cy5 is responsible for the inhibition of gene expression and for fluorescence imaging, is represented schematically in Figure 1a. Dynamic light scattering (DLS) analysis shows that the hydrodynamic size of the BSA-coated MnMEIO nanoparticle increases from 30 nm to 50 and 75 nm in MnMEIO–siGFP–Cy5 and MnMEIO–siGFP–Cy5/PEG–RGD, respectively (Figure 1b). The zeta potential also changes upon conjugation from −5 mV for MnMEIO to −35 and −30 mV for MnMEIO–siGFP–Cy5 and MnMEIO–siGFP–Cy5/PEG–RGD, respectively. The increase in size and decrease in zeta-potential values are the consequence of the presence of highly negatively charged siRNA molecules on the nanoparticle surface. These observations provide evidence for the successful conjugation of siRNA molecules onto the surface of MnMEIO nanoparticles. A parallel trend is also apparent in the results of a gel electrophoresis experiment (Figure 1c). The average number of surface-bound siRNA molecules on each nanoparticle was 40 ± 1, as estimated on the basis of a PicoGreen assay after cleavage of the disulfide bonds between siRNA and the nanoparticles with dithiothreitol (DTT). The nanoparticles are highly stable in an aqueous suspension and retain their colloidal stability in the presence of NaCl at a concentration of up to 500 mM at pH 5–9 (Figure 1d). Importantly, the relatively small size of the nanoparticles and the negative charges may aid in the reduction of nonspecific cellular uptake and enhance the efficiency with which cancer cells are targeted.

To confirm the specific cellular-targeting ability of these nanoparticles, their affinity for breast-cancer cells (MDA-MB-435) that express $\alpha_v\beta_3$ integrin and lung-carcinoma cells (A549) deficient in $\alpha_v\beta_3$ integrin was evaluated (Figure 2a). Each cell line was treated with the MnMEIO–siGFP–Cy5/PEG–RGD nanoparticles (0–4 pmol) and then imaged simultaneously by MRI and fluorescence confocal microscopy. In the *T2**-weighted gradient echo MR images at 3.0 T for $\alpha_v\beta_3$ integrin positive MDA-MB-435 cells, MR contrasts were strong and became more intense with increasing amounts of the nanoparticles (Figure 2b). In comparison, no change in MR contrast was observed for receptor-deficient A549 cells. The MRI signals respond in a proportional manner to the amount of modified nanoparticles present, which shows that nonspecific binding to the cells does not occur. The $1/T2$ values corresponding to the addition of 0, 2, and 4 pmol of the nanoparticles were 0.00071, 0.00129, and 0.00199 ms^{-1} for MDA-MB-435 cells, whereas no difference was observed in the $1/T2$ values for A549 cells regardless of whether or not the nanoparticles were present (Figure 2c). The results of the MRI study clearly show that the RGD-conjugated nanoprobes bind specifically to the targeted cells. The color-coded MR images based on $1/T2$ also show this behavior (Figure 2b).

For accurate information to be attained on the subcellular distribution of nanoparticles, fluorescence imaging, which can identify the locations of the nanoparticles on a micrometer scale, is essential. It is known that a specific interaction between $\alpha_v\beta_3$ integrin and RGD peptides induces intracellular internalization by endocytosis.[11] Because of the

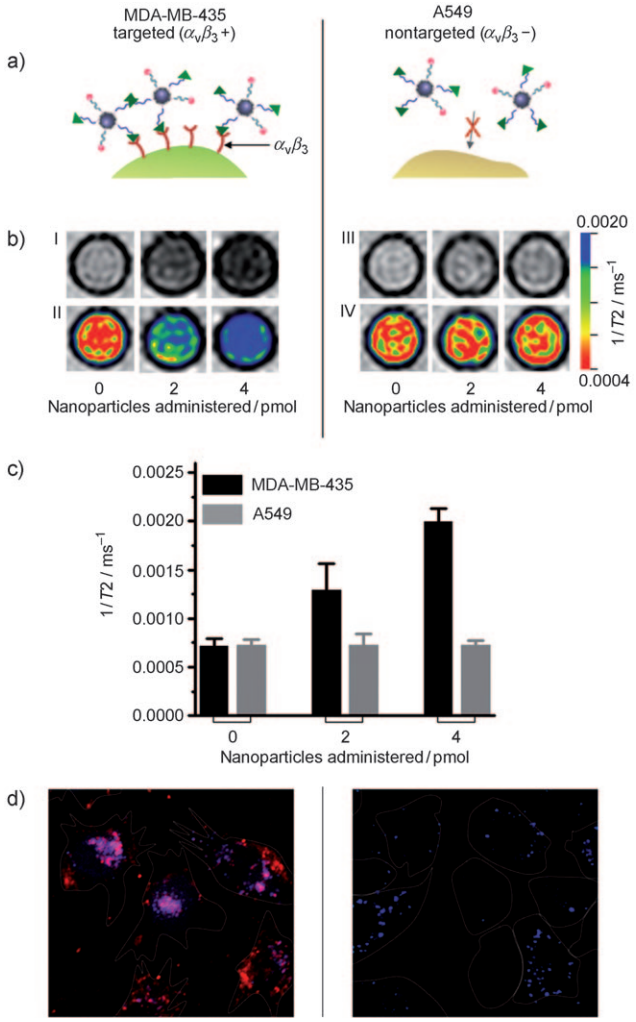

Figure 2. Magnetic resonance and fluorescence imaging of the multimodal nanoparticle system. a) Schematic illustration of the target-specific binding of the nanoparticle to $\alpha_v\beta_3$ integrin positive cells. b) *T2**-weighted MR images and their color maps of I,II) MDA-MB-435 and III,IV) A549 cells treated with MnMEIO–siGFP–Cy5/PEG–RGD. Red corresponds to untreated cells and nanoparticle-treated A549 cells, and green and green-blue correspond to treated MDA-MB-435 cells. c) Values 1/*T2* for cells treated with an increasing amount of nanoparticles. d) Confocal microscopy images showing the distribution of MnMEIO–siGFP–Cy5/PEG–RGD nanoparticles in cells. Nanoparticles appear red, endosomes stained with lysotracker appear blue, merged red and blue regions appear pink. The cell morphology is outlined on the images.

fluorescent Cy5 dye component of the MnMEIO–siGFP–Cy5/PEG–RGD nanoparticles, the internalization of nanoparticles into receptor-positive MDA-MB-435 cells could be visualized clearly; a strong red fluorescence was observed, whereas no red fluorescence was observed with the receptor-deficient A549 cells (Figure 2d). The confocal microscope images also revealed that a considerable amount of siRNA escaped from the endosome into the cytoplasm area of MDA-MB-435 cells. Thus, optical imaging can be very beneficial for the study of targeted siRNA delivery.

The important function of MnMEIO–siGFP–Cy5/PEG–RGD nanoparticles is their use in the targeted delivery of anticancer gene therapeutics. To probe this feature, we undertook a model study to investigate the gene suppression of GFP. In this study, we used MDA-MB-435-GFP and A549-GFP cells that overexpress GFP endogenously. MnMEIO–siGFP–Cy5/PEG–RGD nanoparticles were transfected into the cells under the same conditions as those used in the MRI and fluorescence imaging experiments described above. MnMEIO–siGFP–Cy5/PEG nanoparticles without RGD peptides were used as controls for cellular transfection. For the $\alpha_v\beta_3$ integrin positive cell line (MDA-MB-435-GFP), a significant reduction in the intensity of green fluorescence was observed upon treatment with MnMEIO–siGFP–Cy5/PEG-RGD nanoparticles (Figure 3a, top, middle), whereas no notable reduction in the fluorescence signal was observed when the receptor-deficient control cell line (A549-GFP) was treated with the nanoparticles (Figure 3a, bottom, middle).

The results clearly demonstrate the RGD-mediated target-gene-silencing effects of the nanoparticles. To gain additional evidence in support of the conclusion that target-specific gene inhibition occurs in this system, MnMEIO–siGFP–Cy5/PEG nanoparticles that lack RGD peptides were probed. In both receptor-positive and receptor-negative cell lines, no noticeable changes in the fluorescence signal were observed upon treatment with MnMEIO–siGFP–Cy5/PEG nanoparticles lacking the RGD peptide (Figure 3a, right). The corresponding level of GFP expression was quantified by luminescence spectroscopy. When the amount of MnMEIO–siGFP–Cy5/PEG–RGD was increased from 2 pmol to 4 and 6 pmol, the relative intensity of GFP fluorescence from the cells decreased from 83% to 65 and 67%, respectively, for $\alpha_v\beta_3$ integrin positive MDA-MB-435-GFP cells (Figure 3b). In contrast, no significant change in the level of GFP expression was observed for $\alpha_v\beta_3$ integrin negative A549 cells when the amount of RGD-containing nanoparticles was increased (Figure 3b). As expected, no change in fluorescence occurred upon treatment with MnMEIO–siGFP–Cy5/PEG nanoparticles lacking RGD in both receptor-positive and receptor-negative cell lines (Figure 3c). In contrast to polyethyleneimine (PEI, MW 25kDa), a popular gene-delivery vector with a well-known "proton sponge" effect, our system clearly demonstrates target-specific gene inhibition (Figure 3b). Although the extent of gene inhibition was approximately 20% lower with the nanoparticles than with PEI, a clear target-cell-specific gene-inhibition effect and reduced toxicity towards cells (see the Supporting Information) relative to that of PEI, which is known to have a severe toxicity problem,[15] give our nanoparticles the potential for good clinical applicability.

A specific interaction between RGD and $\alpha_v\beta_3$ integrin facilitates the entry of the nanoparticles into the cells. Some of the nanoparticles are thought to follow the endolysosomal pathway to escape from the endosome (see the Supporting Information).[9b,14] The observed gene-suppression effect is probably caused by the release of an intact siRNA species through the cleavage of a disulfide linkage between siRNA and the nanoparticle in the intracellular reductive environment in the presence of glutathione.[16] It is known that freed siRNA is incorporated into the RNA-induced silencing complex (RISC) to initiate a posttranscriptional gene-silenc-

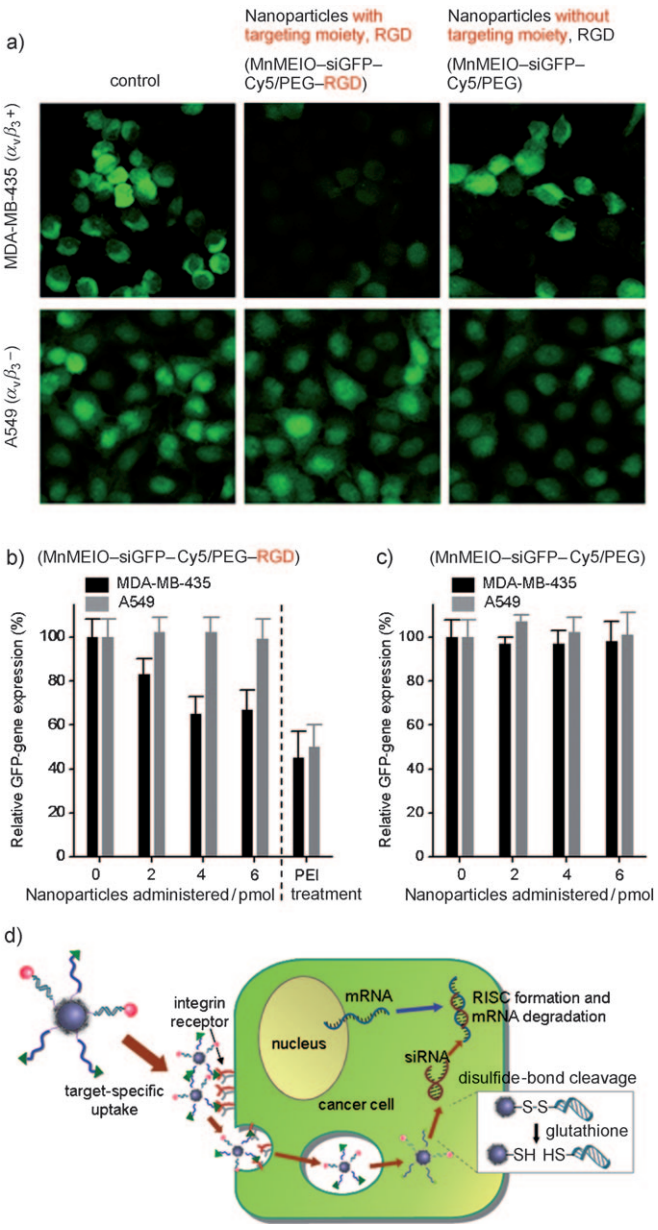

Figure 3. Gene-silencing effect of the multimodal nanoparticle systems with (MnMEIO–siGFP–Cy5/PEG–RGD) and without a targeting moiety (MnMEIO–siGFP–Cy5/PEG) on $\alpha_v\beta_3$ integrin positive (MDA-MB-435) and $\alpha_v\beta_3$ integrin negative (A549) cell lines. a) The levels of GFP fluorescence of MDA-MB-435 and A549 cells that overexpress GFP reliably were visualized by confocal microscopy after treatment with MnMEIO–siGFP–Cy5/PEG–RGD or MnMEIO–siGFP–Cy5/PEG. b,c) Dose-dependent targeted GFP-gene-silencing effect mediated by the interaction of RGD with $\alpha_v\beta_3$ integrin in MDA-MB-435 and A549 cells that overexpress GFP. Cells were treated with MnMEIO–siGFP–Cy5/PEG–RGD and with MnMEIO–siGFP–Cy5/PEG as a negative control. The GFP-expression level of nontreated cells was set as 100%, and the gene silencing of PEI-treated cells is shown for comparison. d) Schematic illustration of intracellular processes involving MnMEIO–siGFP–Cy5/PEG–RGD nanoparticles, from target-specific uptake to mRNA degradation.

ing pathway in the cytoplasm (see Figure 3d). Thus, the cleavable bonds between the nanoparticles and siRNA appear to be essential for the induction of an RNA-interference (RNAi) mechanistic cascade without hindering the formation of the siRNA/RISC complex sterically. Recently, Derfus et al. emphasized the importance of a cleavable disulfide bond in the gene-silencing efficiency of siRNA conjugated to nanoparticles; they found two- to fivefold enhancements in gene silencing relative to results with a noncleavable thioether bond.[9b] In general, an environmentally sensitive bond on the nanocarrier, that is, a bond that is cleaved by an enzyme or at a particular pH value, is known to enhance the efficiency of the intracellular delivery process.[17]

A TEM study of MDA-MB-435 cells treated with MnMEIO–siGFP–Cy5/PEG–RGD nanoparticles provided detailed information on the spatial distribution of nanoparticles within the cells. The nanoparticles (black dots in red circles) were distributed in the endosome and cytoplasm 40 h after treatment in a ratio of 7:3 with respect to the two locations (Figure 4I, II, III); none were found in the nucleus (Figure 4IV). In contrast, nanoparticles were not detected either inside or on the surface of $\alpha_v\beta_3$ integrin deficient A549 cells (see Figure S1 in the Supporting Information). The

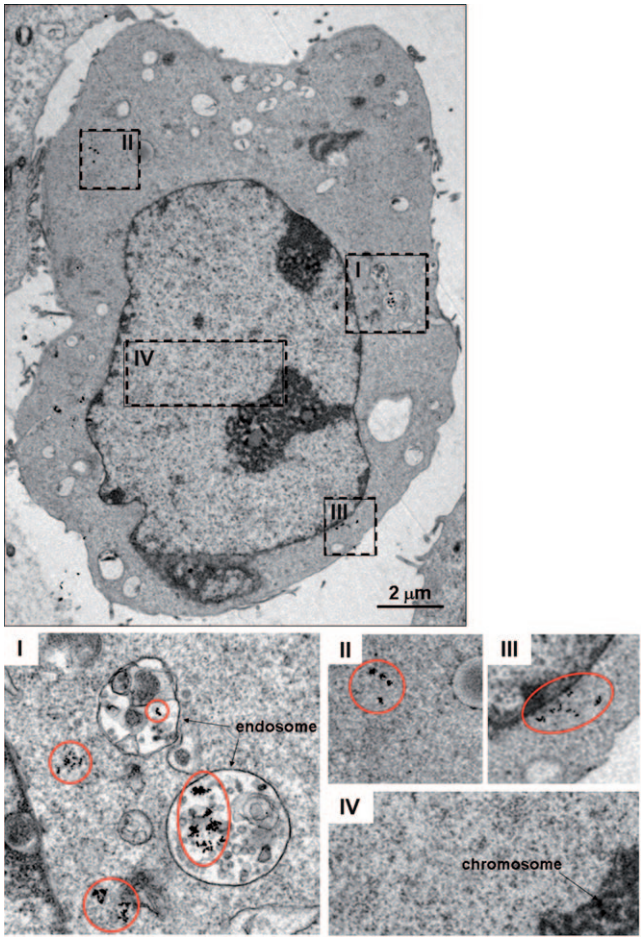

Figure 4. Analysis by transmission electron microscopy (TEM) of the intracellular fate of the multimodal nanoparticle system (MnMEIO–siGFP–Cy5/PEG–RGD) administered to MDA-MB-435 cells. Images I–IV are magnified sections of the above TEM image: I) endosome, II,III) cytoplasm, IV) nucleus. The black dots inside the red circles are nanoparticles.

nanoparticle distribution is consistent with observations in the fluorescence confocal microscopy study (see Figure 2d).

Even though nanoparticle delivery to the cytoplasm is important, the exact mechanisms are still unclear.[18] There are a number of factors that can affect successful nanoparticle delivery to the cytoplasm. For example, it has been reported that the aid of specific peptides or proteins is important.[10c–e] In our specific case, it is highly likely that nanoparticle delivery to the cytoplasm from the endosome is associated with the endolysosomal pathway.[14] As we observed above, a coating of BSA with a pI value of 6.1 on the nanoparticles seems to facilitate their delivery to the cytoplasm. Under physiological buffer conditions (pH ≈ 7), nanoparticles would have a negative charge. However, under acidic endolysosomal conditions (pH ≈ 5), nanoparticle surfaces would be positively charged, which results in enhanced nanoparticle fusion with the endosomal membrane and subsequent escape.

In this study, we have demonstrated multifunctional "all-in-one" magnetic nanoparticles comprising a cell-specific targeting moiety, a fluorescent dye, and therapeutic siRNA in one system. We expect the following potential advantages for future in vivo and clinical applications: 1) The multivalency of the nanoparticles could be beneficial for accommodating a variety of functional groups, so that the nanoparticles could be potentially beneficial as an advanced multimodal nanoplatform; 2) cell-specific targeting moieties and an antibiofouling polymer, such as PEG, should be useful for the specific targeting of cancer cells and reduce unwanted organ uptake, for example, by the liver or spleen;[19] 3) most importantly, simultaneous diagnosis and therapeutic treatment, so-called theragnosis, will minimize invasiveness and side effects.

Experimental Section

Preparation of the nanoparticles: BSA-stabilized nanoparticles were synthesized by a previously described method with the following slight modification:[20] BSA was cationized by chemical modification with 2,2′-(ethylenedioxy)bis(ethylamine); the cationized BSA had a pI value of about 6.1.[13] BSA-stabilized MnMEIO nanoparticles were functionalized with thiolated PEG–RGD (MW 3400) and thiolated siRNA–Cy5 by using the cross-linker SPDP: The heterofunctional PEG derivative NH_2–PEG–COOH (20 mg, Sunbio) was treated with *N*-succinimidyl *S*-acetylthioacetate (SATA; 2 mg, Pierce, Rockford, IL) for 2 h and desalted for purification. Purified SATA–PEG was treated with a cyclic RGD peptide (10 mg, Peptides International) and 1-ethyl-3-(3-dimethylaminopropyl)carbodiimide (EDC; 8 mg, Sigma) for 2 h. SATA-protected PEG–RGD was then treated with 0.5 M hydroxylamine in 50 mM sodium phosphate (pH 7.5) for 2 h, and the product, HS–PEG–RGD, was purified by using HiTrap desalting columns (GE Healthcare). siRNA that had been modified with a thiol group at the 3′ end and labeled with Cy5 at the 5′ end (HS–siRNA–Cy5) was synthesized by Bioneer Co. (Daejeon, Korea). Prior to conjugation, thiol-modified siRNA was incubated with a 50 mM dithiothreitol (DTT) solution for 2 h, and excess DTT was removed by using a dextran desalting column (Pierce). For the conjugation of HS–siRNA–Cy5 and HS–PEG–RGD to the MnMEIO nanoparticles through disulfide linkages, the amino groups of the BSA-coated iron oxide nanoparticles (1 mg) were activated with SPDP (0.2 mg). The SPDP-modified MnMEIO nanoparticles (0.015 nmol) were resuspended in 10 mM phosphate-buffered saline (PBS; pH 7.5) and treated with a 0.6-fold excess of HS–PEG–RGD or thiolated PEG and thiolated siRNA (2 equiv) for 36 h. The resulting solution was filtered through an Amicon Ultra-4 filter (molecular-weight cutoff 100kDa, Millipore) and resuspended in the 10 mM PBS solution. This step was repeated seven times to remove any remaining PEG–RGD or siRNA. To measure the amount of conjugated siRNA, the filtered particles were incubated with 100 mM DTT for 2 h to cleave the disulfide bonds between the siRNA and the particles, and the siRNA was assayed by using the PicoGreen assay (Molecular Probes) according to the recommendations of the suppliers.

Cell culture: MDA-MB-435-GFP ($\alpha_v\beta_3$ +) and A549-GFP cells ($\alpha_v\beta_3$ −) that reliably overexpress GFP were obtained from Samyang Co. (Daejeon, Korea). The cells were cultivated in Dulbecco modified Eagle medium (Invitrogen, Carlsbad, CA) supplemented with 10% fetal bovine serum (FBS; Invitrogen), penicillin (100 units mL^{-1}), and streptomycin (100 ug mL^{-1}) at 37 °C under a humidified 5% CO_2 atmosphere.

Fluorescence imaging: Cy5-labeled MnMEIO–siGFP–Cy5/PEG–RGD (2 and 4 pmol) was added to 1×10^4 cells cultured in a cell-culture-chamber slide for 2 h under serum-free conditions. The cells were washed with PBS solution three times and fixed with 1% formaldehyde. The fixed cells were imaged by confocal laser scanning microscopy (LSM 510, Carl Zeiss).

Magnetic resonance imaging: MDA-MB-435 and A549 cells were treated with MnMEIO–siGFP–Cy5/PEG–RGD (2 and 4 pmol). The nanoparticles were added to 1×10^4 cells cultured in a 12-well culture slide for 30 min under serum-free conditions. Each well was washed with PBS solution three times, and the cells were detached by using trypsin/ethylenediaminetetraacetic acid (EDTA). The detached cells were fixed with 4% formaldehyde and imaged with a 3.0 T clinical MRI instrument with a micro-47 surface coil (Philips Achieva). *T2**-weighted MR images were obtained at room temperature. The following parameters were used: fast spin-echo mode, point resolution: 391 μm × 391 μm, section thickness: 1.0 mm, TE = 100 ms, TR = 4000 ms, number of acquisitions: 2.

Gene suppression: To investigate targeted inhibition of the GFP gene by MnMEIO–siRNA–Cy5/PEG–RGD, siRNA that selectively suppresses the GFP gene was used. MDA-MB-435-GFP cells and A549-GFP cells were seeded in a cell-culture-chamber slide or 12-well plate at a density of 1×10^4 cells per well and cultured for 24 h prior to transfection. The medium was then replaced with a serum-free medium containing MnMEIO–siGFP–Cy5/PEG–RGD at various concentrations, and cells were incubated for 4 h. After transfection, the treated cells were incubated for a further 40 h in culture medium and then washed with PBS solution three times. The washed cells were fixed with 1% formaldehyde for confocal microscopy and lysed with 1% triton X-100 for quantitative measurement of the level of GFP fluorescence. The fixed cells were visualized with a confocal laser scanning microscope (LSM 510, Carl Zeiss), and the relative level of GFP expression in the cell lysate was measured quantitatively by using a spectrofluorophotometer (SLM-AMINCO 8100, SLM Instruments, Rochester, NY) at excitation and emission wavelengths of 488 and 520 nm, respectively. The level of GFP fluorescence was normalized to the total cellular protein content, which was determined by a micro BCA (bicinchoninic acid) assay (Pierce). TEM was used to evaluate the location and amount of MnMEIO–siGFP–Cy5/PEG–RGD taken up into the cells through the RGD–$\alpha_v\beta_3$ integrin interaction. To quantify the nanoparticle distribution in organelles, the nanoparticles in seven different cells were counted by TEM analysis.

Received: December 9, 2008
Published online: April 30, 2009

Keywords: drug delivery · magnetic nanoparticles · magnetic resonance imaging · multimodal imaging · siRNA

[1] a) C. M. Niemeyer, C. A. Mirkin, *Nanobiotechnology*, Wiley-VCH, Weinheim, **2004**; b) S. M. Moghimi, A. C. Hunter, J. C. Murray, *FASEB J.* **2005**, *19*, 311 – 330.

[2] a) Y. W. Cao, R. Jin, C. A. Mirkin, *Science* **2002**, *297*, 1536 – 1540; b) X. Michalet, F. F. Pinaud, L. A. Bentoilla, J. M. Tsay, S. Doose, J. J. Li, G. Sundaresan, A. M. Wu, S. S. Gambhir, S. Weiss, *Science* **2005**, *307*, 538 – 544; c) D. Putnam, *Nat. Mater.* **2006**, *5*, 439 – 451; d) J. N. Anker, W. P. Hall, O. Lyandres, N. C. Shah, J. Zhao, R. P. Van Duyne, *Nat. Mater.* **2008**, *7*, 442 – 453; e) X. Qian, X.-H. Peng, D. O. Ansari, O. Yin-Goen, G. Z. Chen, D. M. Shin, L. Yang, A. N. Young, M. D. Wang, S. Nie, *Nat. Biotechnol.* **2008**, *26*, 83 – 90.

[3] a) Y.-X. J. Wang, S. M. Hussain, G. P. Krestin, *Eur. Radiol.* **2001**, *11*, 2319 – 2331; b) Q. A. Pankhurst, J. Connolly, S. K. Jones, J. Dobson, *J. Phys. D* **2003**, *36*, R167 – R181; c) L. LaConte, N. Nitin, G. Bao, *Nano Today* **2005**, *8*, 32 – 38; d) J. Dobson, *Drug Dev. Res.* **2006**, *67*, 55 – 60.

[4] a) N. Wang, J. P. Butler, D. E. Ingber, *Science* **1993**, *260*, 1124 – 1127; b) A. Tibbe, B. de Grooth, J. Greve, P. Liberti, G. Dolan, L. Terstappen, *Nat. Biotechnol.* **1999**, *17*, 1210 – 1213; c) R. Weissleder, A. Moore, U. Mahmood, R. Bhorade, H. Benveniste, E. A. Chiocca, J. P. Basilion, *Nat. Med.* **2000**, *6*, 351 – 354; d) M. W. Wilson, R. K. Kerlan, N. A. Fidleman, A. P. Venook, J. M. LaBerge, J. Koda, R. L. Gordon, *Radiology* **2004**, *230*, 287 – 293; e) Y. K. Hahn, Z. Jin, J. H. Kang, E. Oh, M.-K. Han, H.-S. Kim, J.-t. Jang, J.-H. Lee, J. Cheon, S. H. Kim, H.-S. Park, J.-K. Park, *Anal. Chem.* **2007**, *79*, 2214 – 2220; f) J.-P. Fortin, C. Wilhelm, J. Servais, C. Ménager, J.-C. Bacri, F. Gazeau, *J. Am. Chem. Soc.* **2007**, *129*, 2628 – 2635.

[5] a) J.-H. Lee, Y.-w. Jun, S.-I. Yeon, J.-S. Shin, J. Cheon, *Angew. Chem.* **2006**, *118*, 8340 – 8342; *Angew. Chem. Int. Ed.* **2006**, *45*, 8160 – 8162; b) J. Kim, S. Park, J. E. Lee, S. M. Jin, J. H. Lee, I. S. Lee, I. Yang, J.-S. Kim, S. K. Kim, M.-H. Cho, T. Hyeon, *Angew. Chem.* **2006**, *118*, 7918 – 7922; *Angew. Chem. Int. Ed.* **2006**, *45*, 7754 – 7758; c) J. Yang, C.-H. Lee, H.-J. Ko, J.-S. Suh, H.-G. Yoon, K. Lee, Y.-M. Huh, S. Haam, *Angew. Chem.* **2007**, *119*, 8992 – 8995; *Angew. Chem. Int. Ed.* **2007**, *46*, 8836 – 8839; d) M. Nahrendorf, H. Zhang, S. Hembrador, P. Panizzi, D. E. Sosnovik, E. Aikawa, P. Libby, F. K. Swirski, R. Weissleder, *Circulation* **2008**, *117*, 379 – 387.

[6] D. M. Dykxhoorn, D. Palliser, J. Lieberman, *Gene Ther.* **2006**, *13*, 541 – 552.

[7] a) J. Soutschek, A. Akinc, B. Bramlage, K. Charisse, R. Constien, M. Donoghue, S. Elbashir, A. Geick, P. Hadwiger, J. Harborth, M. John, V. Kesavan, G. Lavine, R. K. Pandey, T. Racie, K. G. Rajeev, I. Röhl, I. Toudjarska, G. Wang, S. Wuschko, D. Bumcrot, V. Koteliansky, S. Limmer, M. Manoharan, H. P. Vornlocher, *Nature* **2004**, *432*, 173 – 178; b) P. Kumar, H. Wu, J. L. McBride, K.-E. Jung, M. H. Kim, B. L. Davidson, S. K. Lee, P. Shankar, N. Manjunath, *Nature* **2007**, *448*, 39 – 45.

[8] a) A. Aigner, *Curr. Opin. Mol. Ther.* **2007**, *9*, 345 – 352; b) A. Sanguino, G. Lopez-Berestein, A. K. Sood, *Mini-Rev. Med. Chem.* **2008**, *8*, 248 – 255.

[9] a) D. B. Rozema, D. L. Lewis, D. H. Wakefield, S. C. Wong, J. J. Klein, P. L. Roesch, S. L. Bertin, T. W. Reppen, Q. Chu, A. V. Blokhin, J. E. Hagstrom, J. A. Wolff, *Proc. Natl. Acad. Sci. USA* **2007**, *104*, 12982 – 12987; b) A. M. Derfus, A. A. Chen, D. H. Min, E. Ruoslahti, S. N. Bhatia, *Bioconjugate Chem.* **2007**, *18*, 1391 – 1396; c) Z. Medarova, W. Pham, C. Farrar, V. Petkova, A. Moore, *Nat. Med.* **2007**, *13*, 372 – 377; d) S. H. Lee, S. H. Choi, S. H. Kim, T. G. Park, *J. Controlled Release* **2008**, *125*, 25 – 32; e) A. Akinc, A. Zumbuehl, M. Goldberg, E. S. Leshchiner, V. Busini, N. Hossain, S. A. Bacallado, D. N. Nguyen, J. Fuller, R. Alvarez, A. Borodovsky, T. Borland, R. Constien, A. de Fougerolles, J. R. Dorkin, K. N. Jayaprakash, M. Jayaraman, M. John, V. Koteliansky, M. Manoharan, L. Nechev, J. Qin, T. Racie, D. Raitcheva, K. G. Rajeev, D. W. Sah, J. Soutschek, I. Toudjarska, H. P. Vornlocher, T. S. Zimmermann, R. Langer, D. G. Anderson, *Nat. Biotechnol.* **2008**, *26*, 561 – 569.

[10] a) L. LaConte, N. Nitin, G. Bao, *Mater. Today* **2005**, *8*, 32 – 38; b) J. Cheon, J.-H. Lee, *Acc. Chem. Res.* **2008**, *41*, 1630 – 1640; c) C. Plank, B. Oberhauser, K. Mechtler, C. Koch, E. Wagner, *J. Biol. Chem.* **1994**, *269*, 12918 – 12924; d) A. G. Tkachenko, H. Xie, D. Coleman, W. Glomm, J. Ryan, M. F. Anderson, S. Franzen, D. L. Feldheim, *J. Am. Chem. Soc.* **2003**, *125*, 4700 – 4701; e) S. H. Lee, S. H. Kim, T. G. Park, *Biochem. Biophys. Res. Commun.* **2007**, *357*, 511 – 516.

[11] a) W. Arap, R. Pasqualini, E. Ruoslahti, *Science* **1998**, *279*, 377 – 380; b) J. Enback, P. Laakkonen, *Biochem. Soc. Trans.* **2007**, *35*, 780 – 783; c) M. Oba, S. Fukushima, N. Kanayama, K. Aoyagi, N. Nishiyama, H. Koyama, K. Kataoka, *Bioconjugate Chem.* **2007**, *18*, 1415 – 1423.

[12] J.-H. Lee, Y. M. Huh, Y. Jun, J.-w. Seo, J.-t. Jang, H. T. Song, S. Kim, E.-J. Cho, H. G. Yoon, J. S. Suh, J. Cheon, *Nat. Med.* **2007**, *13*, 95 – 99.

[13] G. T. Hermanson, *Bioconjugate Techniques*, Academic Press, San Diego, **1996**.

[14] a) J. Panyam, W.-Z. Zhou, S. Prabha, S. K. Sahoo, V. Labhasetwar, *FASEB J.* **2002**, *16*, 1217 – 1226; b) S. Prabha, V. Labhasetwar, *Pharm. Res.* **2004**, *21*, 354 – 364.

[15] T. G. Park, J. H. Jeong, S. W. Kim, *Adv. Drug Delivery Rev.* **2006**, *58*, 467 – 486.

[16] a) E. P. Feener, W.-C. Shen, H. J.-P. Ryser, *J. Biol. Chem.* **1990**, *265*, 18780 – 18785; b) S. H. Kim, J. H. Jeong, S. H. Lee, S. W. Kim, T. G. Park, *J. Controlled Release* **2006**, *116*, 123 – 129.

[17] a) E. R. Gillies, J. M. J. Fréchet, *Chem. Commun.* **2003**, 1640 – 1641; b) Y. Bae, S. Fukushima, A. Harada, K. Kataoka, *Angew. Chem.* **2003**, *115*, 4788 – 4791; *Angew. Chem. Int. Ed.* **2003**, *42*, 4640 – 4643.

[18] a) D. Putnam, *Nat. Mater.* **2006**, *5*, 439 – 451; b) H. Duan, S. Nie, *J. Am. Chem. Soc.* **2007**, *129*, 3333 – 3338; c) A. El-Sayed, I. A. Khalil, K. Kogure, S. Futaki, H. Harashima, *J. Biol. Chem.* **2008**, *283*, 23450 – 23461.

[19] M. K. Yu, Y. Y. Jeong, J. Park, S. Park, J. W. Kim, J. J. Min, K. Kim, S. Jon, *Angew. Chem.* **2008**, *120*, 5442 – 5445; *Angew. Chem. Int. Ed.* **2008**, *47*, 5362 – 5365.

[20] J.-s. Choi, J. C. Park, H. Nah, S. Woo, J. Oh, K. M. Kim, G. J. Cheon, Y. Chang, J. Yoo, J. Cheon, *Angew. Chem.* **2008**, *120*, 6355 – 6358; *Angew. Chem. Int. Ed.* **2008**, *47*, 6259 – 6262.

